www.lajss.org
Latin American Journal of Solids and Structures 1 (2003) 25–47

Numerical simulation of large deformation of flat-topped conical shells made of textile composite

R.H. Bao[a,b], P. Xue[a,c], T.X. Yu[a,*] and X.M. Tao[c]

[a]Department of Mechanical Engineering, Hong Kong University of Science and Technology, Hong Kong
[b]Department of Mechanics, Zhejiang University, Hangzhou, P.R. China
[c]Institute of Textiles and Clothing, The Hong Kong Polytechnic University, Hong Kong

Abstract

This paper numerically analyzes the large deformation behaviour of a grid-domed textile composite consisting of flat-topped conical cells under quasi-static axial compression. Based on experimental observations and previous theoretical analysis, a pair of small transverse forces applied at the appropriate opposite positions of the conical cell is introduced as the initial imperfection to stimulate the diamond-pattern deformation-mode of an anisotropic cell. The geometric changes of the cell and the contact conditions of the displacement-controlled axial compression process are taken into simulation. The numerical results are found in good agreement with experimental results and theoretical analysis in the deformation-mode and the load-carrying capacity. With the verified FE model, the effects of geometric parameters and other factors on the energy absorption capacity of conical cells are examined, so some local optimal parameters are obtained.

Keywords: Flat-topped conical shell, Cellular textile composite, Energy absorption capacity, Finite element simulation

1 Introduction

Over the last several decades the energy absorption capacity of numerous materials (metals, polymers, foams and composites etc.) and structural components (rings, thin-walled tubes, conical frusta and frames etc.) has been investigated for various purposes in engineering applications. It is evident that the energy absorption capacity of a structure depends on the material properties as well as the deformation modes of the structure under the specified loading condition. As summarized by Johnson and Reid [3] and Yu [9], an energy absorption structure should utilise the inelastic deformation (plastic deformation, friction, and fracture etc.) as its energy dissipation mechanism; the load required for its large deformation should remain almost constant, while the deformation should be in a stable and repeatable mode, allowing a long

* Corresponding author Email: metxyu@ust.hk Received 4 Sep 2003

stroke. In addition to these requirements, the structure weight is also an important factor in many engineering applications.

With the advances in composite technology, more research attention has been paid to the energy absorption capacity of composite structures, including textile composites, under impact loads. Typical textile composite components being studied include braided composite I-beams as crushing elements in cars, triaxially braided composite square tubes as crushing elements and 3-D woven sandwich structures. As well known, one-dimensional or cross-layered fibre-reinforced composites possess higher specific strength and stiffness compared with conventional isotropic materials; whilst textile composites exhibit distinct advantage in their energy absorption capacity. For the latter, the reinforced fibers, the matrix and the fibre architecture, as well as the fabrication process can be optimised to improve the mechanical properties of the composite, to monitor the structure's deformation mode, so as to achieve a desired energy absorption capacity.

On the other hand, cellular materials and structures, due to their light weight, a large amount of deformable space, easy fabrication and high energy absorption capacity, have been widely used as energy absorbers or cushions to resist dynamic loads. Previous studies were mainly focused on metal ring systems, tube arrays, honeycombs, polymer foams and wood.

Combining the advantages of textile composite and cellular structures, in the last few years, we have developed a range of cellular textile composites with high specific energy absorption capacity and stable deformation mode. In particular, the experimental and theoretical studies [4–7, 10] have been conducted for gird-domed textile composites with two cell configurations. The first configuration has a hemispherical dome connected to a truncated conical shell. The second configuration consists of flat-topped conical cells. The quasi-static axial compression and impact tests were carried out, and the energy absorption capacities for these two configurations were compared and analysed. Based on our experimental observations, the large deformation mode of flat-topped conical shells under quasi-static axial compression was identified and modelled, leading to a good agreement with experimental results.

It would be too costly and inconvenient, however, to conduct experimental studies for all possible combinations of material and geometric parameters. Meanwhile, the validity of simplified theoretical models is restricted by either linear elasticity or rigid-plastic idealization. Thus, a numerical simulation is required to gain a full understanding of the large deformation behaviour of grid-domed textile composites. Finite element method is applied to determine the cell's configuration and to optimise the structural parameters, so as to significantly save time and cost in the design of this kind of energy absorbers.

In this paper, the large deformation process of a textile composite conical shell under quasi-static axial compression is numerically simulated, while a pair of small transverse forces is employed as the initial imperfection to approximately account for the effect of the anisotropy of the material. The load-displacement curve and energy absorption capacity obtained from the FE analysis are then compared with experimental results and theoretical models' predictions. Finally, the influences of geometric parameters and other conditions on the energy absorption capacity are examined.

2 Experimental Results and Theoretical Analysis

The reinforcements of the grid-domed textile composites used in this study were 1×1 interlock knitted fabrics made of textured nylon multi-filament yarns, produced in our laboratory. The flat fabrics were formed into a 3D cellular structure by a two-step method. The flat fabrics were placed into a mould and deformed into in a grid pattern, whilst each cell comprised a flat-topped conical shell. This was followed by heat setting treatment in the mould at 200°C for 5 minutes, then cooling down to ambient temperature. Polyester resin was used with 1% methylethyl ketone peroxidie (MEKP) as the initiator and 0.5% cobalt naphthenate as the accelerator. The textile preforms were coated with this mixture, and then cured at room ambient conditions.

In order to characterize the mechanical properties of the nylon/polyester textile composite, flat composite samples with identical percentage of resin added-on, which had been rigidified by the same process as the grid-domed cellular composites, were used for tests under tension and compression. The samples were cut along the wale and course directions, respectively. For simple tension test, samples with the size of 200mm×20mm×1mm were elongated at a crosshead speed of 5mm/min. For uniaxial compression test at loading speed of 1mm/min, relatively short (gauge length 15mm), multi-plies samples, with two ends embedded in epoxy resin, were used to prevent global buckling. The applied load and the displacement were recorded in both tension and compression tests. The stress-strain curves are plotted in Fig. 1, from which the required material properties are determined.

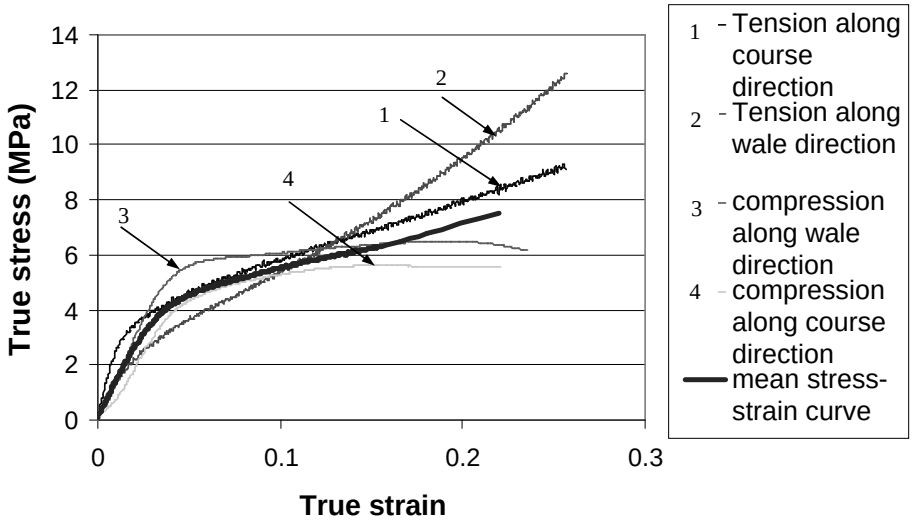

Figure 1: True stress-strain curves of the textile materials obtained from tension and compression tests.

Quasi-static compression tests for grid-domed composites were carried out on an MTS Testing machine with a crosshead speed of 1mm/min until the cells were fully compressed. Each

sample had an area of $20cm^2$ containing 4 complete conical cells. During the test, the samples were compressed axially between two parallel thick steel flat platens. Figure 2 shows a typical sample before and after axially compression, while Fig. 3 provides the front and side views of a cell after partially compressed and springback. It is evident that a two-lobe diamond pattern deformation mode was formed. Figure 4 records the deformation process and the geometric details by a series of photographs taken from the top, side and front of a sample.



(a) (b)

Figure 2: (a) A typical sample before compressed; (b) A typical sample after compressed.



Figure 3: A typical cell after partly compressed, taken from front and side.

Based on experimental observations, a large deformation mechanism was identified. An elastic model and a rigid-linear hardening plastic model were proposed to predict the load-

displacement characteristics in the early and later stages, respectively, of the large elastic-plastic deformation process. Within the plastic stage, the deformation model possesses plastic hinge lines along the top and bottom circles, as well as along a horizontal loop (refer to [6] and [7]). The bending along plastic hinge lines and the stretching of the thin-wall segments between the plastic hinge lines both are incorporated into the analysis of the model, so that the load-displacement relationships and energy-absorption behaviour during the large deformation process are calculated. A good agreement has been achieved between the theoretical predictions and experimental results [7].

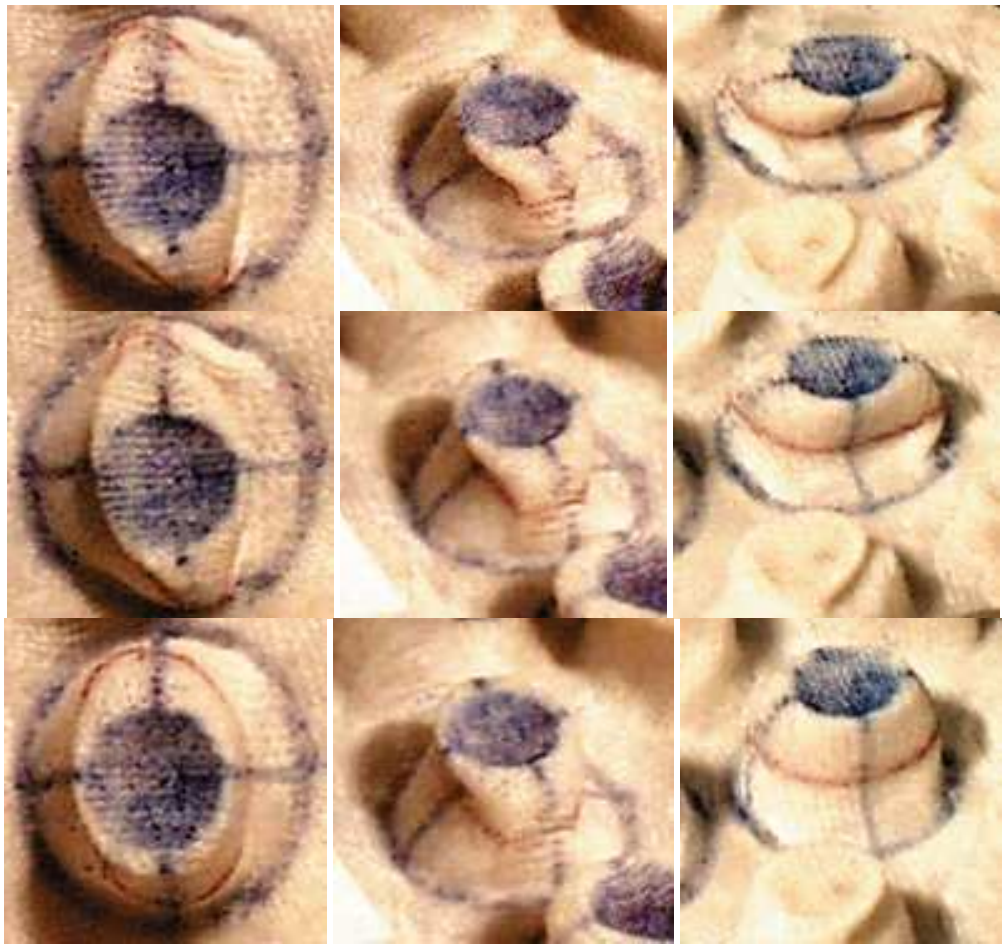

Figure 4: The deformation process taken from the top, side and front of a cell.

3 FE model

The following parameters and methods are employed in simulating the large deformation process of a flat-topped conical shell.

3.1 Material behaviour

The knitted textile composite investigated is anisotropic and it is difficult to determine the principal directions of the material after it has been formed into the shape of conical cells. Nevertheless, as the deformation mode of such a structure is concerned, the material is regarded as isotropic in the first-order approximation, whilst appropriate imperfections is introduced either in geometry or in loading condition to account for effect caused by the anisotropy of the material.

For simplicity, the classical plasticity model is adopted in our FE model, which employs the von Mises yield surface to define the isotropic yielding and isotropic strain hardening. Based on the strain-stress curves experimentally obtained from the knitted textile composite samples along three different orientations (wale, course and 45° inclination) [8], the average material properties used in FE calculations are

Young's modulus	E =136 MPa
Poisson ratio	$\nu = 0.35$
Yield stress	$Y = 4.5$ MPa
Hardening modulus	$E_p = 15$ MPa

3.2 Geometric parameters and meshes

Unless specified, the geometric parameters of a cell are taken as

Diameter of the top circle	$D_1 = 10$mm
Diameter of the bottom circle	$D_2 = 18$mm
Diameter of the bottom outskirt	$D_3 = 24$mm
Shell wall thickness	$t = 0.9$mm
Shell height	$h = 13.8$mm
Fillet radius at the top	$R_1 = 1.5$mm
Fillet radius at the bottom	$R_2 = 3.0$mm

Here the shell wall-thickness is determined by a bending test and it is thus slightly different from the direct measurement. Since the surface of the textile composite sheet is not as smooth as that of metal sheets, the effective thickness used in calculation is indeed smaller than the thickness measured.

The cross section of a cell is shown in Fig. 5. A quarter of a cell is meshed in the FE

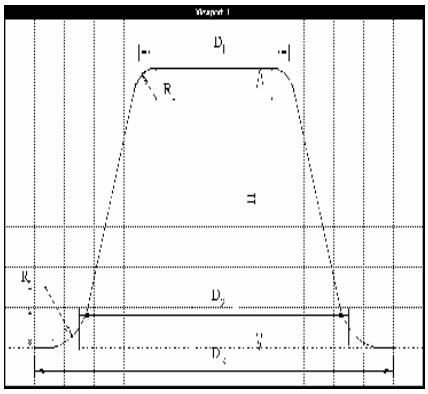

Figure 5: Cross section of a cell.

model and is depicted in Fig. 6 which includes all the meshes in our model except the two rigid surfaces, the top and the bottom of the conical shell. The nodes in the XY and YZ planes should be restricted by boundary conditions, which are symmetric to the XY plane and the YZ plane, respectively. A quarter of the conical shell is discreterised into approximately 900 S4R shell elements in ABAQUS, which are 4-node, double curved thin or thick shell elements with reduced integration, hourglass control and finite membrane strain. The number of integration points in the S4R elements is 5.

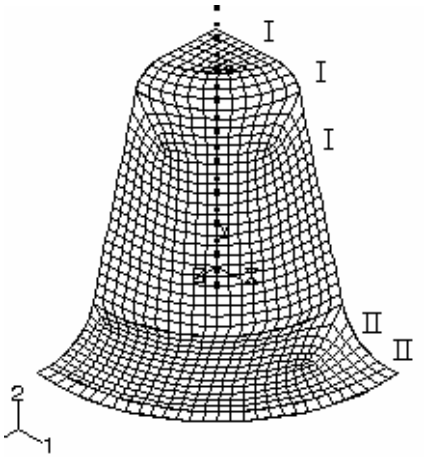

Figure 6: Mesh of the FE model.

3.3 Contact condition

Since the tested samples were compressed between two rigid flat plates, when the top surface of the shell moved down, the contact boundaries at the top and bottom surfaces would change

accordingly. Hence, some nodes may lose contact with the plates while some other nodes may come into contact with the plates. In our FE model, the plates are modelled as rigid surfaces; and two hard-contact pairs are defined: one is defined between the top plate and region I of the cell, while the other is defined between the bottom plate and region II of the cell (see Fig. 6). The tangential friction on these two contact pairs is neglected for numerical simplicity.

3.4 Riks analysis

A load-displacement analysis method, called Riks method [1], is adopted in our pre-buckling and post-buckling analyses to overcome the difficulties caused by the material and geometric non-linearities in the pre-buckling analysis of thin-wall structures and/or the unstable and negative global stiffness appeared in the post-buckling response. In the method the displacement magnitude is used as an additional unknown, while the load and displacement are solved simultaneously regardless of the stable or unstable response. The plate supporting the bottom surface of the shell is supposed to be fixed, while the displacement of the plate at the top surface is regarded as "live displacement", whose minimal and maximal incremental values in Riks analysis methods are set as 0.1 mm and 1.0mm, respectively.

3.5 Initial transverse forces

From our experimental observation, the plastic hinge lines were formed along the top and bottom circles of a cell, as well as along a horizontal circumferential loop at about two third of the cell height, resulting in two rhombuses on the front and back surfaces of the cell [6] (see Figs. 2 and 3). On the other hand, it is known from our trial calculations that when the cell is made by perfectly isotropic material with the properties specified above, the conical shell will yield first at about two third of the height and then fold outwards in the vicinal areas almost axisymmetrically. By considering the anisotropic properties of the textile composite, therefore, it is reasonable to introduce a pair of small transverse compressing forces, with the same magnitude but opposite directions, acting at the appropriate opposite positions of the cell wall, while these positions are approximately determined by the trial calculations. However, the magnitude of this pair of initial transverse forces is very crucial. If the forces are too small, the shell will not deform into a two-lobe diamond pattern; but if the forces are too large, the error caused by the initial forces may be significant. The effect of the magnitude of the initial transverse forces on the calculation results will be discussed later.

3.6 Boundary condition on the bottom surface

Two kinds of boundary conditions at the edge of the bottom surface, which connects the neighbouring cells, are examined in the FE model; that is, a free boundary and a symmetric boundary. Here the "symmetric boundary" means that the displacements and rotations of the nodes at the edge of the bottom surface should be symmetric to the cylindrical surfaces formed by the

circle of this edge. The free boundary condition represents the case in which only one single cell is compressed; while the symmetric boundary condition approximately represents the case in which multi-cells are compressed as an entire piece of sample. The deformation mode and load-carrying capacity under these two kinds of boundary conditions will be compared later.

3.7 Solution controls in non-linear equation

Large deformation theory, variable contact conditions and material nonlinearlity are all included in our FE models, resulting in a severe non-linear problem.

Because the contact constraints could switch between present and absent at a particular point on the top and bottom surfaces, a discontinuous behaviour occurs in our FE model. Therefore, "CONTROL, ANALYSIS=DISCONTINUOUS" option should be included in the FE model to allow relatively large amount of iterations prior to starting any convergence rate check, which usually improves the efficiency for severely discontinuous behaviour.

Meanwhile, because the rotation angle corrections are not much smaller than the rotation angle increments in calculation, the increment may not converge within specified iterations [1]. Therefore, it is useful to relax the tolerance on the residual moment (R_n^α and C_n^α) by including an ABAQUS option "*CONTROLS, PARAMETERS=FIELD, FIELD=ROTATION".

4 Results of Finite Element Simulation

4.1 Comparison with experimental and theoretical results

As illustrated above, the first step in the simulation is to select the location and magnitude of the initial transverse forces. Based on the experimental observations, the conical shell had plastic hinge lines formed along a horizontal circumferential loop at about two third of the height, resulting in a two-lobe diamond pattern deformation mode. Therefore, it is assumed that the initial transverse force is applied at the node located at $y = 9.90$mm, while its direction is along the negative z-axis. As the numerical results indicate, when the initial force approaches 2.8N, a diamond deformation pattern begins to occur. Through the Riks analysis method, the deformation process is given in Fig. 7. The left and right pictures of Fig. 7 are taken from the negative z-direction and the negative x-direction, respectively. It agrees well with the deformation process demonstrated by the photographs taken in the experiments (Fig. 4).

Figure 8 depicts the load-displacement curves obtained from the FE simulation, experiment and theoretical analysis [6]. It can be seen that the numerical result essentially lies between the theoretical and experimental results. The discrepancy between the numerical result and experimental result is attributed to many factors, such as the approximation of isotropic properties, the measurement error of material's properties, the effect of micro-crack when the textile composite experienced large strains, the approximation of effective wall-thickness, and so on. However, the numerical result does provided good predictions for the peak load and the flat sec-

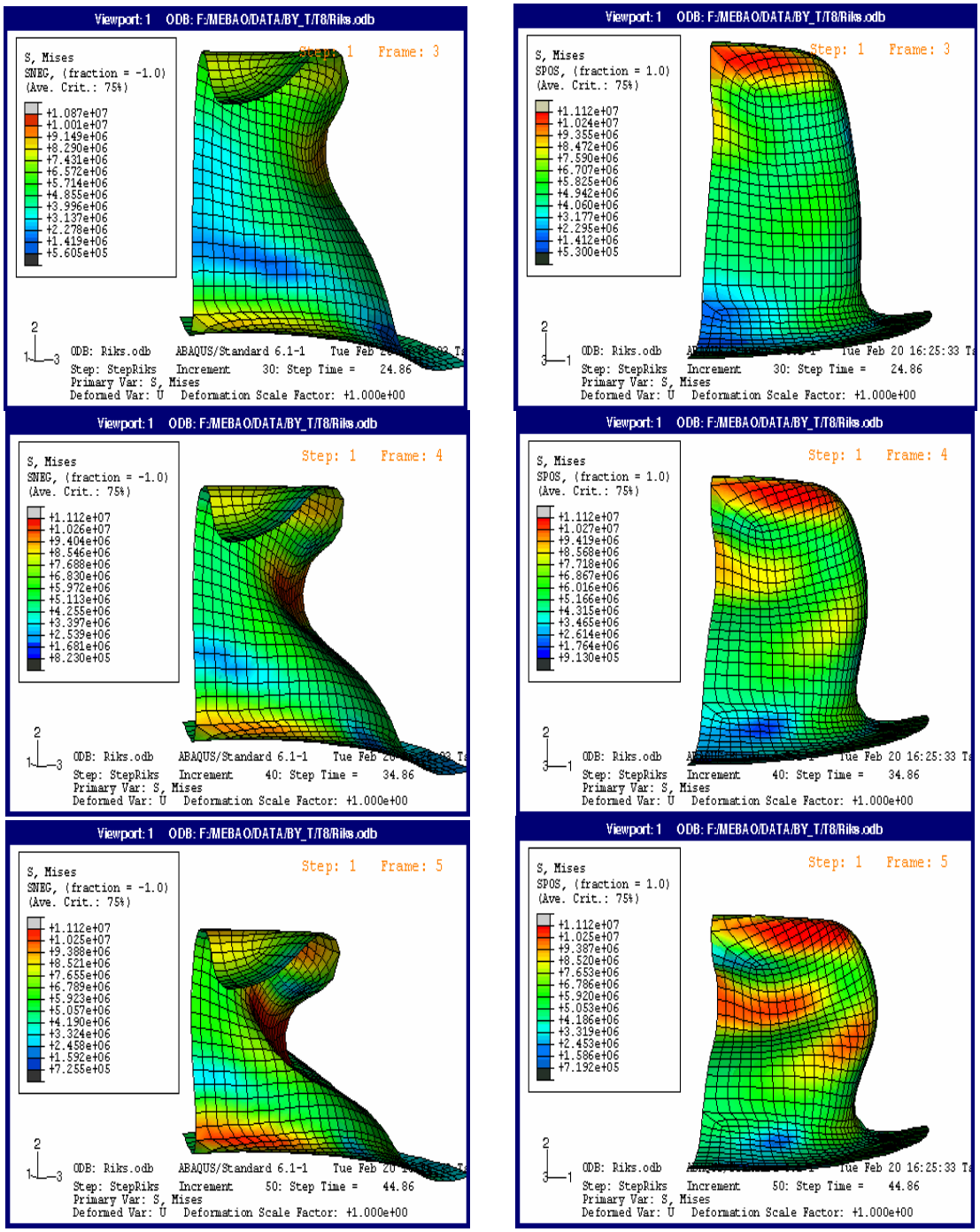
Viewport: 1 ODB: F:/MEBAO/DATA/BY_T/T8/Riks.odb
S, Mises
SNEG, (fraction = -1.0)
(Ave. Crit.: 75%)
+1.087e+07
+1.001e+07
+9.149e+06
+8.290e+06
+7.431e+06
+6.572e+06
+5.714e+06
+4.855e+06
+3.996e+06
+3.137e+06
+2.278e+06
+1.419e+06
+5.605e+05
Step: 1 Frame: 3
ODB: Riks.odb ABAQUS/Standard 6.1-1
Step: StepRiks Increment 30: Step Time = 24.86
Primary Var: S, Mises
Deformed Var: U Deformation Scale Factor: +1.000e+00
Viewport: 1 ODB: F:/MEBAO/DATA/BY_T/T8/Riks.odb
S, Mises
SPOS, (fraction = 1.0)
(Ave. Crit.: 75%)
+1.112e+07
+1.024e+07
+9.355e+06
+8.472e+06
+7.590e+06
+6.707e+06
+5.825e+06
+4.942e+06
+4.060e+06
+3.177e+06
+2.295e+06
+1.412e+06
+5.300e+05
Step: 1 Frame: 3
ODB: Riks.odb
Step: StepRiks Increment 30: Step Time = 24.86
Primary Var: S, Mises
Deformed Var: U Deformation Scale Factor: +1.000e+00
Viewport: 1 ODB: F:/MEBAO/DATA/BY_T/T8/Riks.odb
S, Mises
SNEG, (fraction = -1.0)
(Ave. Crit.: 75%)
+1.112e+07
+1.026e+07
+9.404e+06
+8.546e+06
+7.688e+06
+6.830e+06
+5.972e+06
+5.113e+06
+4.255e+06
+3.397e+06
+2.539e+06
+1.681e+06
+8.230e+05
Step: 1 Frame: 4
ODB: Riks.odb ABAQUS/Standard 6.1-1
Step: StepRiks Increment 40: Step Time = 34.86
Primary Var: S, Mises
Deformed Var: U Deformation Scale Factor: +1.000e+00
Viewport: 1 ODB: F:/MEBAO/DATA/BY_T/T8/Riks.odb
S, Mises
SPOS, (fraction = 1.0)
(Ave. Crit.: 75%)
+1.112e+07
+1.027e+07
+9.419e+06
+8.568e+06
+7.718e+06
+6.867e+06
+6.016e+06
+5.166e+06
+4.315e+06
+3.465e+06
+2.614e+06
+1.764e+06
+9.130e+05
Step: 1 Frame: 4
ODB: Riks.odb
Step: StepRiks Increment 40: Step Time = 34.86
Primary Var: S, Mises
Deformed Var: U Deformation Scale Factor: +1.000e+00
Viewport: 1 ODB: F:/MEBAO/DATA/BY_T/T8/Riks.odb
S, Mises
SNEG, (fraction = -1.0)
(Ave. Crit.: 75%)
+1.112e+07
+1.025e+07
+9.388e+06
+8.521e+06
+7.655e+06
+6.789e+06
+5.923e+06
+5.057e+06
+4.190e+06
+3.324e+06
+2.458e+06
+1.592e+06
+7.255e+05
Step: 1 Frame: 5
ODB: Riks.odb ABAQUS/Standard 6.1-1
Step: StepRiks Increment 50: Step Time = 44.86
Primary Var: S, Mises
Deformed Var: U Deformation Scale Factor: +1.000e+00
Viewport: 1 ODB: F:/MEBAO/DATA/BY_T/T8/Riks.odb
S, Mises
SPOS, (fraction = 1.0)
(Ave. Crit.: 75%)
+1.112e+07
+1.025e+07
+9.387e+06
+8.520e+06
+7.653e+06
+6.786e+06
+5.920e+06
+5.053e+06
+4.186e+06
+3.319e+06
+2.453e+06
+1.586e+06
+7.192e+05
Step: 1 Frame: 5
ODB: Riks.odb
Step: StepRiks Increment 50: Step Time = 44.86
Primary Var: S, Mises
Deformed Var: U Deformation Scale Factor: +1.000e+00

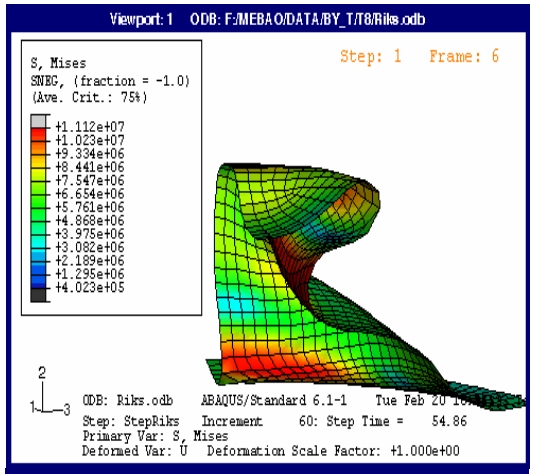
Viewport: 1 ODB: F:/MEBAO/DATA/BY_T/T8/Riks.odb
S, Mises
SNEG, (fraction = -1.0)
(Ave. Crit.: 75%)
+1.112e+07
+1.023e+07
+9.334e+06
+8.441e+06
+7.547e+06
+6.654e+06
+5.761e+06
+4.868e+06
+3.975e+06
+3.082e+06
+2.189e+06
+1.295e+06
+4.023e+05
Step: 1 Frame: 6
ODB: Riks.odb ABAQUS/Standard 6.1-1
Step: StepRiks Increment 60: Step Time = 54.86
Primary Var: S, Mises
Deformed Var: U Deformation Scale Factor: +1.000e+00

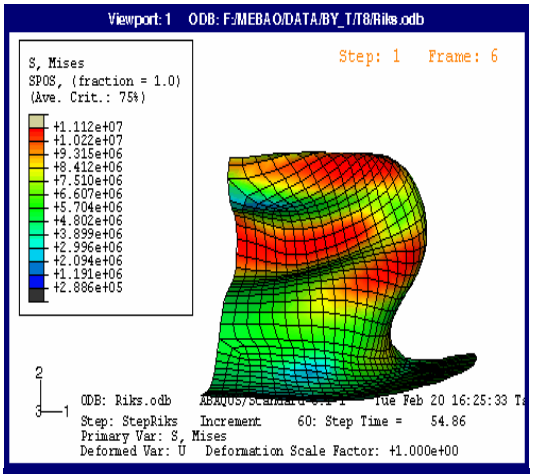
Viewport: 1 ODB: F:/MEBAO/DATA/BY_T/T8/Riks.odb
S, Mises
SPOS, (fraction = 1.0)
(Ave. Crit.: 75%)
+1.112e+07
+1.022e+07
+9.315e+06
+8.412e+06
+7.510e+06
+6.607e+06
+5.704e+06
+4.802e+06
+3.899e+06
+2.996e+06
+2.094e+06
+1.191e+06
+2.886e+05
Step: 1 Frame: 6
ODB: Riks.odb
Step: StepRiks Increment 60: Step Time = 54.86
Primary Var: S, Mises
Deformed Var: U Deformation Scale Factor: +1.000e+00

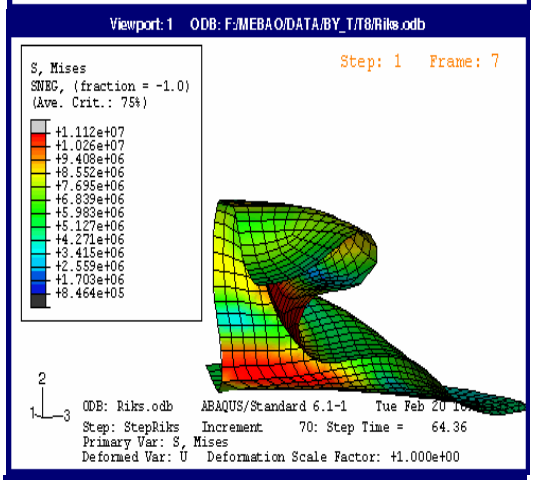
Viewport: 1 ODB: F:/MEBAO/DATA/BY_T/T8/Riks.odb
S, Mises
SNEG, (fraction = -1.0)
(Ave. Crit.: 75%)
+1.112e+07
+1.026e+07
+9.408e+06
+8.552e+06
+7.695e+06
+6.839e+06
+5.983e+06
+5.127e+06
+4.271e+06
+3.415e+06
+2.559e+06
+1.703e+06
+8.464e+05
Step: 1 Frame: 7
ODB: Riks.odb ABAQUS/Standard 6.1-1
Step: StepRiks Increment 70: Step Time = 64.36
Primary Var: S, Mises
Deformed Var: U Deformation Scale Factor: +1.000e+00

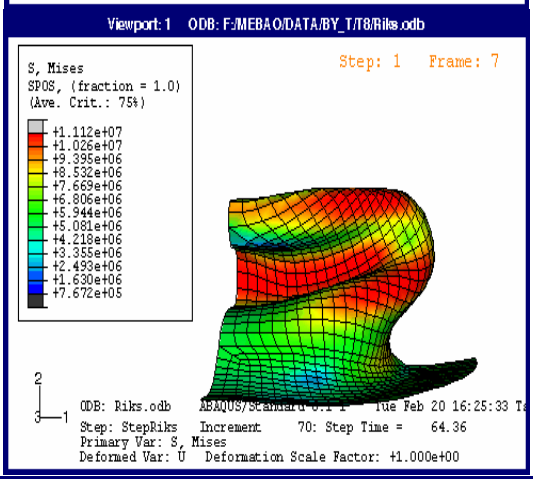
Viewport: 1 ODB: F:/MEBAO/DATA/BY_T/T8/Riks.odb
S, Mises
SPOS, (fraction = 1.0)
(Ave. Crit.: 75%)
+1.112e+07
+1.026e+07
+9.395e+06
+8.532e+06
+7.669e+06
+6.806e+06
+5.944e+06
+5.081e+06
+4.218e+06
+3.355e+06
+2.493e+06
+1.630e+06
+7.672e+05
Step: 1 Frame: 7
ODB: Riks.odb
Step: StepRiks Increment 70: Step Time = 64.36
Primary Var: S, Mises
Deformed Var: U Deformation Scale Factor: +1.000e+00

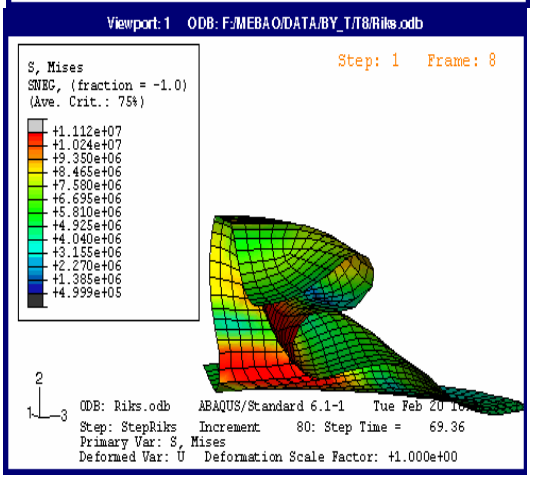
Viewport: 1 ODB: F:/MEBAO/DATA/BY_T/T8/Riks.odb
S, Mises
SNEG, (fraction = -1.0)
(Ave. Crit.: 75%)
+1.112e+07
+1.024e+07
+9.350e+06
+8.465e+06
+7.580e+06
+6.695e+06
+5.810e+06
+4.925e+06
+4.040e+06
+3.155e+06
+2.270e+06
+1.385e+06
+4.999e+05
Step: 1 Frame: 8
ODB: Riks.odb ABAQUS/Standard 6.1-1
Step: StepRiks Increment 80: Step Time = 69.36
Primary Var: S, Mises
Deformed Var: U Deformation Scale Factor: +1.000e+00

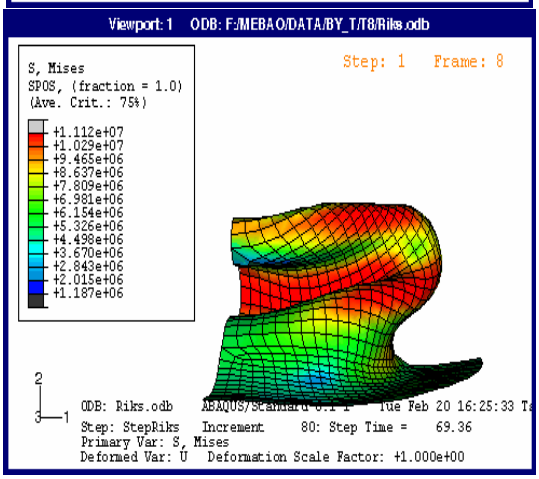
Viewport: 1 ODB: F:/MEBAO/DATA/BY_T/T8/Riks.odb
S, Mises
SPOS, (fraction = 1.0)
(Ave. Crit.: 75%)
+1.112e+07
+1.029e+07
+9.465e+06
+8.637e+06
+7.809e+06
+6.981e+06
+6.154e+06
+5.326e+06
+4.498e+06
+3.670e+06
+2.843e+06
+2.015e+06
+1.187e+06
Step: 1 Frame: 8
ODB: Riks.odb
Step: StepRiks Increment 80: Step Time = 69.36
Primary Var: S, Mises
Deformed Var: U Deformation Scale Factor: +1.000e+00

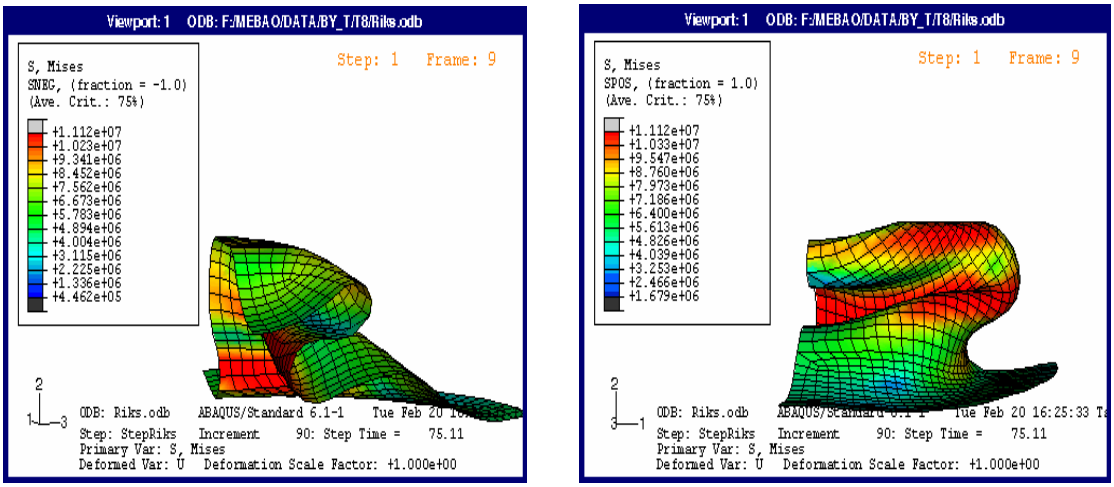

Figure 7: The deformation process of a cell, viewed from side and from front of the FEM model.

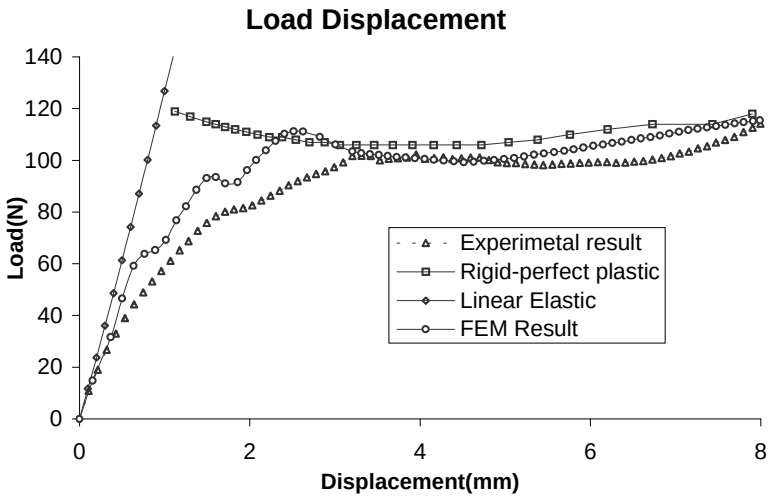

Figure 8: Load-displacement curves for FEM, experimental and theoretical results.

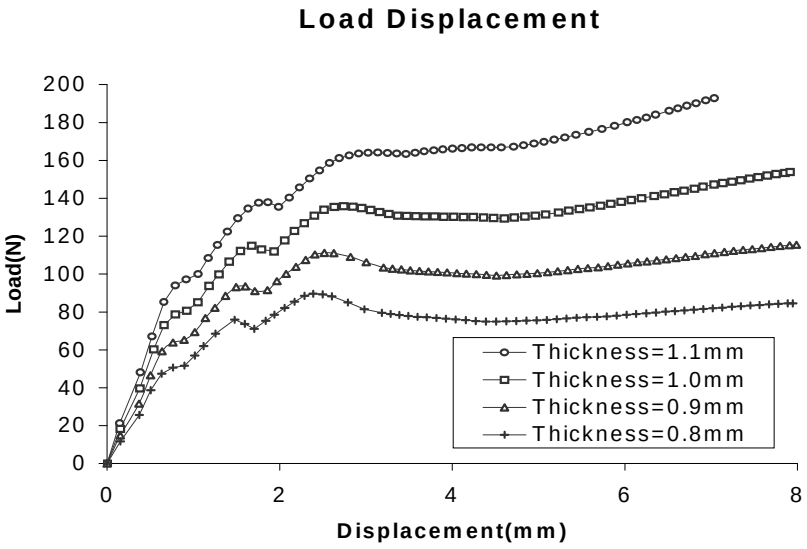

(a)

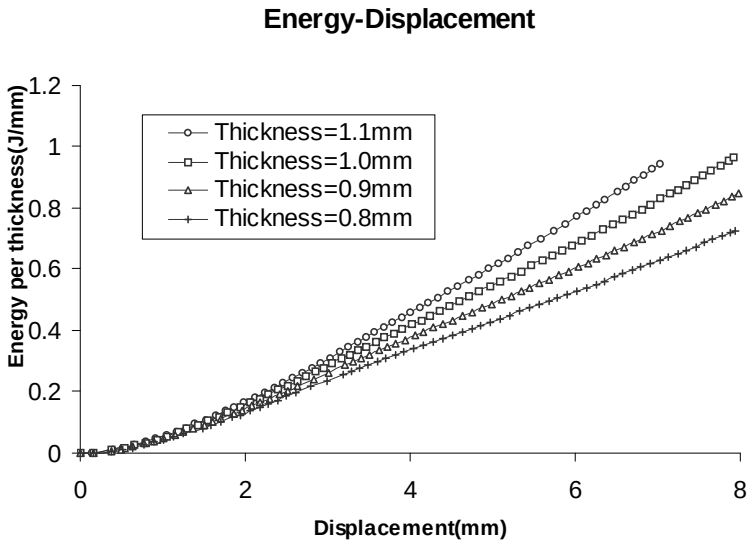

(b)

Figure 9: (a) Load-displacement curves for cells with different thickness; (b) Energy-displacement curves for cells with different thickness.

tion of the stress-strain curve, which both govern the energy absorption capacity of the cellular textile composite. Therefore, it is concluded that such a FE model can be employed to optimise the design parameters of the cellular textile composite in concern, before making samples and conducting verifying experiments.

4.2 Effects of cell geometry

Besides the material properties, the load-carrying capacity and the energy absorption capacity are mainly affected by the geometry of the flat-topped conical cell. The main purpose of our FE simulation is to design more efficient energy absorbers. In the following, the effects of the cell geometric parameters, i.e. the wall-thickness, top-bottom diameter ratio, cell height and apical angle, will be discussed in details.

4.2.1 Effect of wall thickness

The curves of load vs. displacement and energy vs. displacement are depicted in Fig. 9(a) and Fig. 9(b), respectively, for cells with different wall-thickness, while the other geometric parameters remain unchanged. It is evident that the magnitude of the peak load increases from 90N to 164N as the wall thickness varies from 0.8mm to 1.1mm, but the stroke decreases accordingly: the effective displacement decreases from about 8.0mm to 4.0mm. Here the effective displacement is defined as the maximum displacement before the external load exceeds the first peak load, so it is not equal to the maximum displacement before the cell's condensation [2]. This definition is consistent with the final aim of our FE simulation that is to optimise the geometric parameters of the conical cells, with a high energy-absorption capacity and a low peak load. It is seen that the total energy absorbed till this effective displacement remains almost the same for cells with different thickness, but the peak load for thinner cell is much lower and the curve is flatter. Therefore, the cell thickness could be chosen as 0.9mm or thinner in our design.

4.2.2 Effect of cell height

Figures 10(a) and 10(b) depict the load-displacement and energy-displacement curves for the cells with a constant apical angle 16.17°, while the cell thickness is fixed as 0.9mm, the cell height ranges from 15.53mm to 13.11mm, and the radius of the top circle varies from 4.5mm to 5.2mm accordingly. It is evident that the stroke of a higher cell is flatter and longer, and its peak load is smaller. However, a too-high cell will lead to a too-low peak load. From these three cases, it is concluded that if the cell thickness (0.9mm) and the apical angle (16.17^o) are specified, taking the cell height as 15.5mm and the top radius as 4.5mm will make the cell an ideal energy absorber.

Figures 11(a) and 11(b) show the load-carrying capacity and energy absorption capacity of

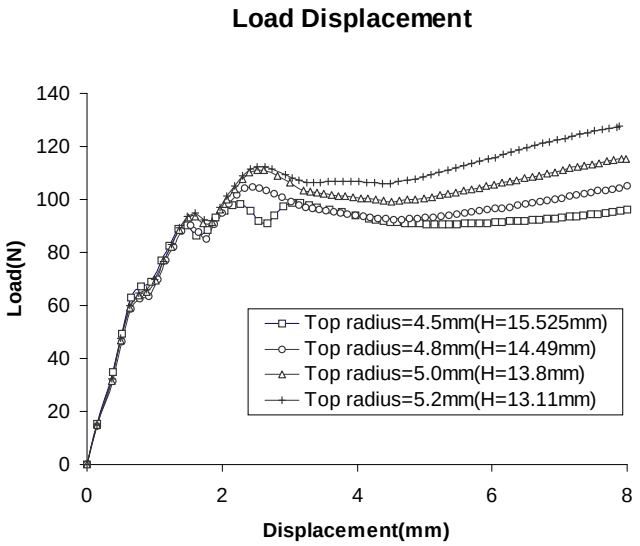

(a)

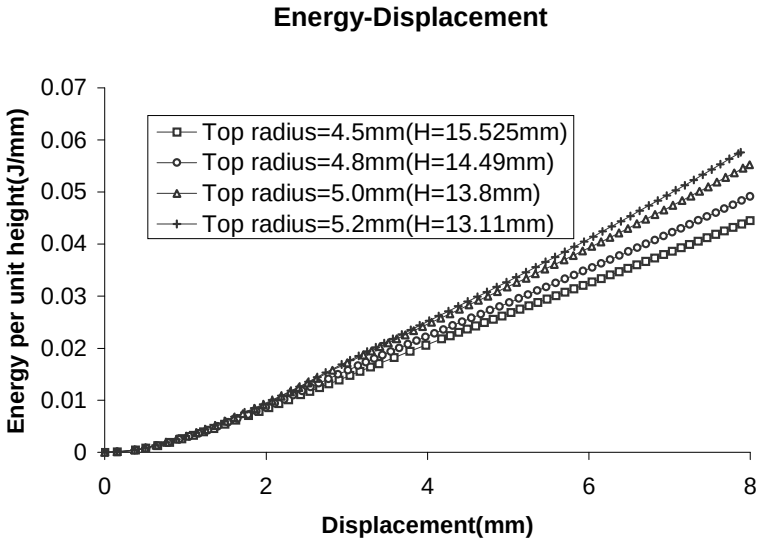

(b)

Figure 10: (a) Load-displacement curves for cells with a constant apical angle of 16.17°; (b) Energy-displacement curves for cells with a constant apical angle of 16.17°.

the cells with a constant top radius of 5.0mm and a constant thickness of 0.9mm, while the height ranges from 12.8mm to 15.8mm. It is clear that the shorter is the cell, the higher is the peak load and the shorter is the stroke. However, if the cell is too high, though the stroke is much flatter and longer, the energy absorption capacity may not be ideal because of the peak load is too low and too much space is wasted. It is seen from these four cases that the ideal cell height would range from 14.8mm to 15.8mm if the top radius remains constant as 5.0mm.

4.2.3 Effect of conical apical angle

Figures 11(a) and 11(b) also show the effect of conical apical angle. Just as discussed in above, when the top radius remains constant as 5.0mm, and the cell height and cell thickness are fixed as 13.8mm and 0.9mm, respectively, a cell with smaller apical angle has a lower peak load accompanied by a flatter and longer stroke. Therefore, the appropriate apical angle may range from 14.21° to 15.13°, while the height varies from 15.8mm to 14.8mm accordingly. When the cell height remains constant, Figs. 12(a) and 12(b) demonstrate the effects of the top radius and conical apical angle. It is evident that the cell with larger top radius has higher peak load. From these three cases, it is seen that the top radius may be taken as 5.0mm, with a corresponding conical apical angle 16.17°.

It is concluded from the above discussions that among all geometric parameters the cell thickness is the most important one, followed by the cell height. Since a global optimisation of cell's geometry is difficult and very costly, in above numerical examples, the selection of the geometrical parameters are limited to some discrete values, which are close to those employed in our experiments.

4.2.4 Effect of boundary conditions

If a sample contains one cell only, the boundary conditions at the edge of the cell's bottom surface should be free. However, if a group of cells works together as a cellular structure, the boundary conditions at the edge of the cell's bottom surface can be approximately regarded as axisymmetric with respect to the cylindrical surface, which is formed by the bottom edge before the cell is compressed. It is evident from the load-displacement curves shown in Fig. 13(a) and the energy-displacement curves shown in Fig. 13(b), the energy absorption capacity of the cell with the axisymmetric boundary condition is about 40% higher than that of a single cell (i.e. the cell with a free boundary condition).

4.3 Effect of the fillets

Figure 14 depicts the load-displacement curves of cells with or without fillets at the top and bottom surfaces. It is evident that the cell without any fillet at the top or the bottom surface has a highest peak load and a shortest stroke, while the cell with fillets at both top and bottom surfaces has a lower peak load and a flatter stroke. Figure 15 shows the load-displacement curves

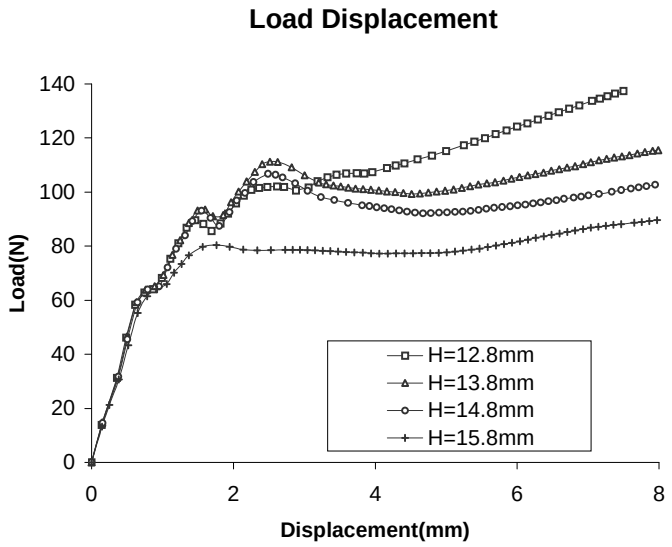

(a)

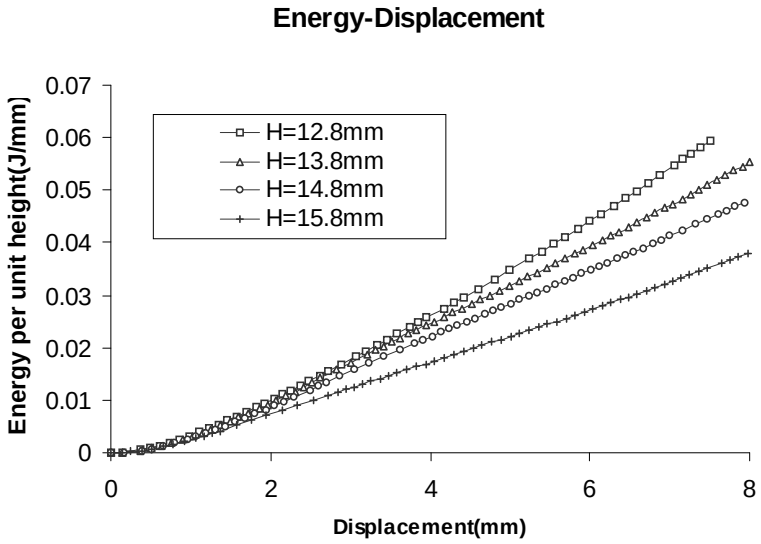

(b)

Figure 11: (a) Load-displacement curves for cells with a constant top radius of 5.0mm; (b) Energy-displacement curves for cells with a constant top radius of 5.0mm.

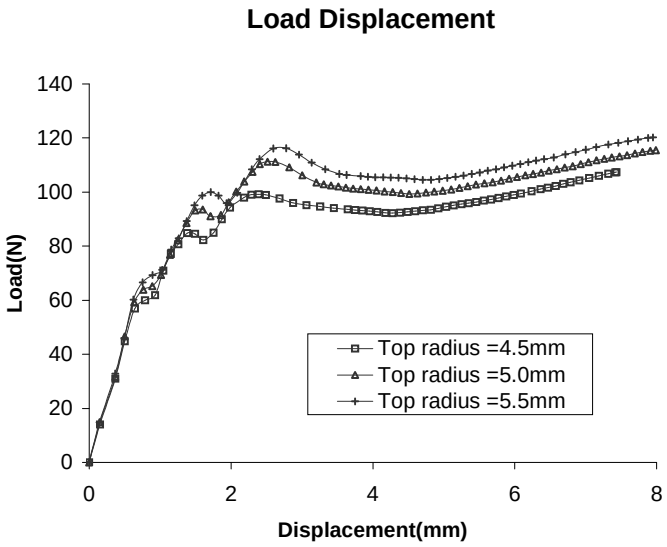

(a)

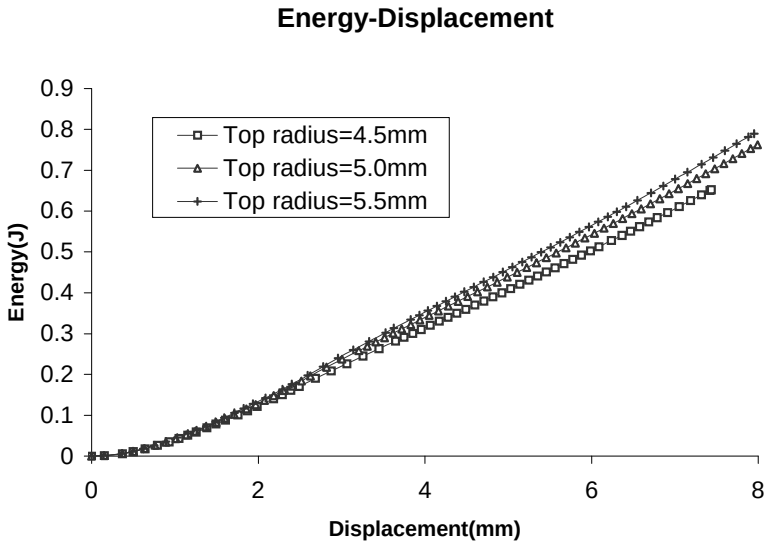

(b)

Figure 12: (a) Load-displacement curves for cells with a constant height of 13.8mm; (b) Energy-displacement curves for cells with a constant height of 13.8mm.

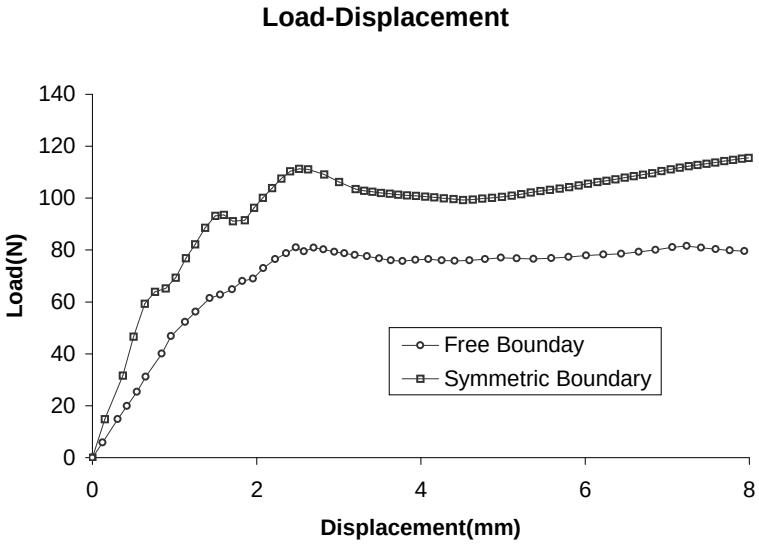

(a)

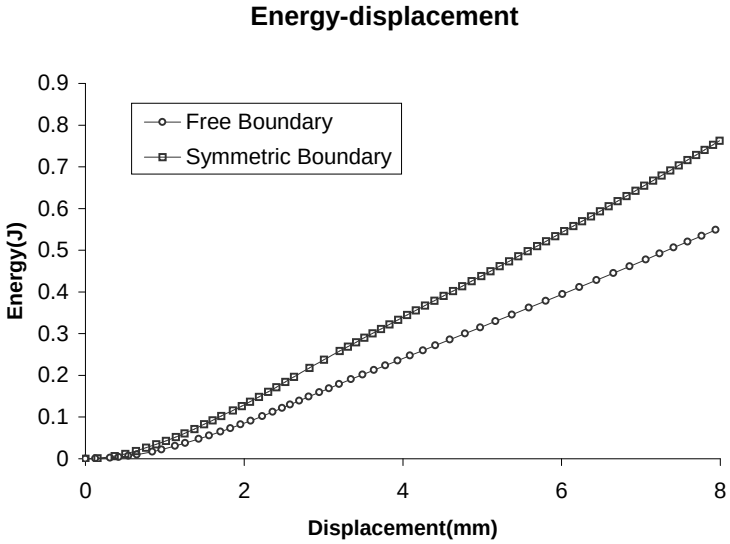

(b)

Figure 13: (a) Load-displacement curves for cells with different boundary conditions; (b) Energy-displacement curves for cells with different boundary conditions.

of cells with different fillet radius at the bottom surface while the fillet radius at the top surface remains constant. It is seen that the load-displacement curves for these three cases are almost identical except a minor difference at the displacement where the peak load occurs.

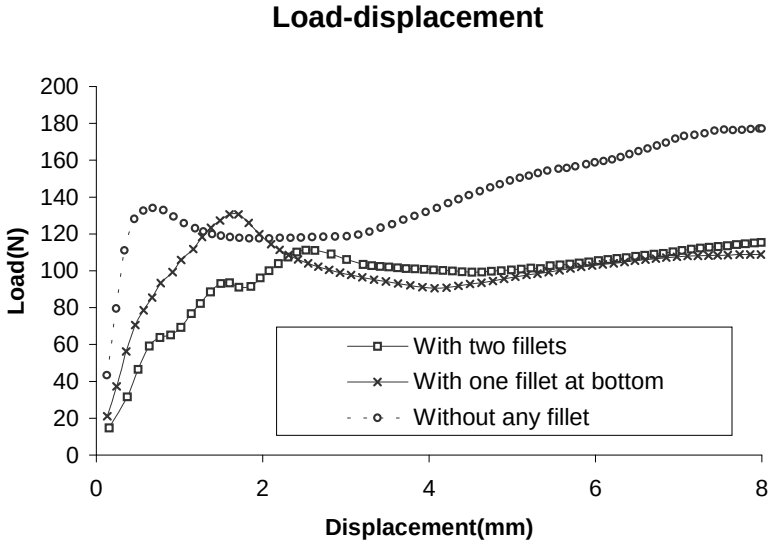

Figure 14: Load-displacement curves for cells with and without fillets.

Therefore, it is necessary to incorporate the fillets at the top and bottom surfaces of a flatted-top conical cell into its FE model in calculation of its energy absorption capacity, although the latter is not very sensitive to the variations of the fillets' radii of the cell under compression.

4.4 Effect of initial transverse forces

If no initial transverse force is applied in the FE simulation, the cell made of an isotropic material would deform axisymmetrically as the cell geometry, loading and boundary condition are all axisymmetric. With appropriate initial transverse forces being applied, however, the FE model of the cell deforms into a diamond pattern, similar to the behaviour observed in the experiment of conical cells made of an anisotropic textile composite. Suppose all parameters of the cell remain the same as listed in Section 3.2, Fig. 16 shows the load-displacement curves obtained from the models with various magnitudes of the initial transverse force. It is obvious that the appropriate initial transverse forces do alter the deformation mode of the cell and make the model behaves more like a cell made of an anisotropic material. It is also observed from Fig. 16 that the influence of a small variation in the initial transverse force on the load-displacement curve is negligible, especially if the energy absorption capacity of the cell is the main concern.

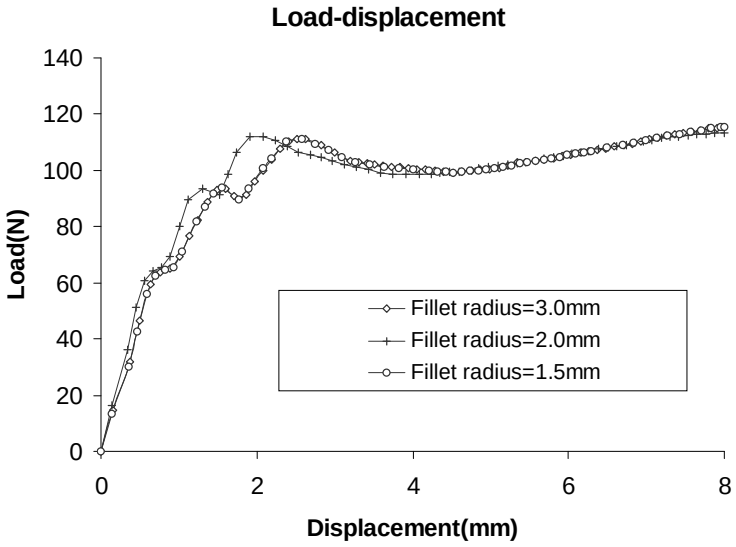

Figure 15: Load-displacement curves for cells with fillets of different radius at the bottom.

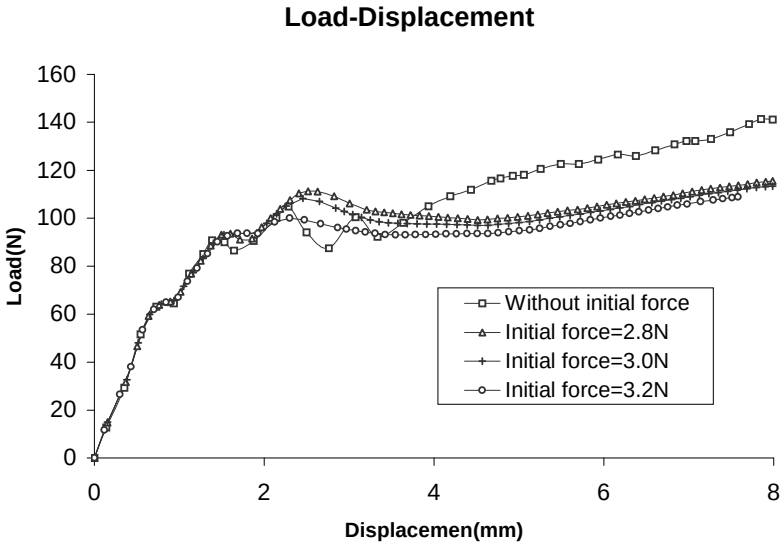

Figure 16: Load-displacement curves of cells with different initial force.

5 Conclusions

A finite element model is established to simulate the large plastic deformation process of a flat-topped conical cell of a cellular textile composite. In the FE model, an initial transverse force is introduced as an initial imperfection to approximately represent the anisotropic behaviour of the material; the contact conditions with two rigid surfaces are implemented in the model to simulate the loading and supporting conditions provided by the two plates used in the experiment; and two fillets at the top and bottom surfaces are incorporated in the model to simulate the real composite cells made by a deep-drawing operation. The large deformation mode and the load-displacement behaviour predicted by the FE model are in good agreement with the experimental results and the predictions from the previous theoretical analysis. The effects of geometric parameters and other factors on the load-displacement behaviour and the energy absorbing capacity are discussed in details. To avoid costly and complex computations, the geometric parameters in the present study are selected only within a local regime around the values employed in our experiments.

Increasing the cell's thickness will raise the peak load under axial compression, but will reduce the stroke. In the parameters' range examined, the ideal effective thickness for our samples would be 0.9mm or thinner. Increasing the cell's height will make the stroke much flatter and longer, but will reduce the peak load significantly. Therefore, the appropriate cell height would be 15.5mm if the apical angle remains as 16°, and it would range between 14.8mm and 15.8mm if the top radius remains as 5.0mm. Increasing the conical apical angle will raise the peak load but shorten the stroke, so that the appropriate apical angle would range from 14° to 15° if the top radius remains as 5.0mm, and it could be taken as 16° if the cell height is taken as 13.8mm. From these results it is evident that the FE models developed in this study are applicable to the parameter design of the cellular textile composites in concern.

Acknowledgments: The authors would like to express their gratitude to the Honk Kong Research Grant Council (RGC) for the financial support under grant HKUST 6017/98E and HKUST 6012/02E. Helpful discussion with Mr. Haihui Ruan is also acknowledged.

References

[1] ABAQUS/Standard User's Manual (Version 6.1). Hibbit, Karlsson & Sorensen, Inc, 2000.

[2] L.J. Gibson and M.F. Ashby. Cellular Solids: Structure and Properties. Cambridge University Press, Cambridge, UK, 2nd edition, 1997.

[3] W. Johnson and S.R Reid. Metallic energy dissipation systems. Appl Mech Rev, pages 277–288, 1977.

[4] S.W. Lam, P. Xue, T.X. Yu, and X.M. Tao. Multi-scale study of tensile properties and large deformation mechanisms of polyethylene terephthalate fibre/polypropylene matrix knitted composites. Composite Science and Technology, 63:1337–1348, 2003.

[5] P. Xue, T.X. Yu, and X.M. Tao. Effect of cell geometry on the energy-absorbing capacity of grid-domed textile composites. Composites Part A - Applied Science and Manufacturing, 31:861–868, 2000.

[6] P. Xue, T.X. Yu, and X.M. Tao. Large deformation model of flat-topped conical shell under axial compression. In T.X. Yu and Q.P. Sun & J.K. Kim, editors, Advances in Engineering Plasticity, pages 745–770. Key Engineering Materials, 2000.

[7] P. Xue, T.X. Yu, and X.M. Tao. Flat-toped conical shell under axial compression. International Journal of Mechanical Science, 43(9):2125–2145, 2001.

[8] P. Xue, T.X. Yu, and X.M. Tao. Tensile properties and meso-scale mechanisms of weft knitted textile composites. Composites Part A – Applied Science and Manufacturing, 33:113–123, 2002.

[9] T.X. Yu. Energy–absorbing device utilizing plastic deformation of metals. Advances in Mechanics, 16(1):28–29, 1987.

[10] T.X. Yu, X.M. Tao, and P. Xue. Energy-absorbing capacity of grid-domed textile composites. Composite Science and Technology, 60(5):755–800, 2000.